Anal. Bioanal. Electrochem., Vol. 15, No. 2, 2023, 118-136
https://www.doi.org/10.22034/abec.2023.702330

Analytical & Bioanalytical Electrochemistry

Full Paper

Omeprazole's Inhibitive Activity on the Corrosion of the Al Alloy in 0.5 M H_2SO_4 Solution

A. Belafhaili,[1] M. El Hawary,[1] A. Bellaouchou,[1] A. Guenbour,[1] I. Warad,[2] and A. Zarrouk[1,*]

[1]*Laboratory of Materials, Nanotechnology and Environment, Faculty of Sciences, Mohammed V University in Rabat, Av. Ibn Battouta, P.O. Box. 1014 Agdal-Rabat, Morocco*
[2]*Department of Chemistry, AN-Najah National University, P.O. Box 7, Nablus, Palestine*

*Corresponding Author, Tel.: +212665201397
E-Mail: azarrouk@gmail.com

Received: 27 December 2022 / Received in revised form: 20 February 2023 / Accepted: 20 February 2023 / Published online: 28 February 2023

Abstract- Potentiodynamic polarization (PDP) and electrochemical impedance spectroscopy (EIS) techniques were used to examine the inhibitory effect of omeprazole (OMP) on the corrosive behavior of Al-Mg-Si alloy in 0.5 M H_2SO_4. SEM/EDS microscopy methods and X-ray diffraction (XRD) analysis were utilized to examine the surface morphology. According to the findings, OMP acted flawlessly as an inhibitor of corrosion for an Al-Mg-Si alloy in 0.5 M H_2SO_4 at 298 K. The effect of temperature on inhibition efficiency was also discussed. Moreover, the experimental results suggest that OMP is an effective inhibitor, with a maximum inhibition efficiency of 90.5% at a concentration of 1.5 g/L, and the potentiodynamic polarization curves show that it is a mixed-type inhibitor. Electrochemical impedance spectroscopy discovered that an inhibitory adsorption film was being formed on the surface of the Al-Mg-Si alloy, and that this adsorption isotherm model is being followed. Thermodynamic activation parameters have been identified and discussed.

Keywords- Aluminium alloy corrosion; Sulfuric acid; Omeprazole; Electrochemical techniques; SEM/EDS/XRD

1. INTRODUCTION

Aluminum alloy has seen an increase in industrial use since its desirable properties were discovered; it is now commonly used as a material in vehicles, aircraft, home appliances, containers, and electronic devices. The rapid formation of oxide films on the surface of aluminum accounts for its resistance to corrosion in aqueous media [1]. However, aluminum corrodes quickly in the presence of corrosive chemicals. This protective coating typically disintegrates and eventually assaults the metal when exposed to acidic environments including pickling, etching, descaling, and oil well acidification. The majority of designed metal components are exposed to chemical attack and exposure, as well as minimal in-service stress conditions [2]. These attacks eventually result in the metal pieces losing their ability to support the design load due to a reduction in effective thickness. The component wastes metal, which prevents it from supporting the appropriate load capacity because it gradually or suddenly loses technical functioning [3].

Because of its benefits, aluminum is an economically significant metal, and its alloys are widely utilized in numerous sectors such as reaction vessels, pipelines, equipment, and chemical batteries. Many writers have concentrated on the investigation of aluminum alloy corrosion in various aqueous solutions. Techniques for preventing and controlling corrosion include applying metallic coatings, cathodic protection, altering the atmosphere, choosing the right materials, and using chemical, organic, and environmentally friendly inhibitors, among others. In the field of corrosion chemistry, there is a growing interest in the development of organic-based aluminum corrosion inhibitors [4].

Several factors such as the electronic structure of the inhibitor molecules, steric factor, aromaticity and electron density at the donor site, as well as the presence of functional groups such as NH, -N = N-, -C = N-, -CHO, R-OH, all have an effect on the adsorption of organic molecules that possess heteroatoms such as phosphorus, nitrogen or sulfur, which are excellent corrosion inhibitors. the inhibitor's molecule's molecular mass and surface area. Adsorption, which results in the formation of a protective film on the metal surface, is the mechanism underlying the inhibition process of these compounds. Due to its biodegradability, environmental friendliness, low cost, and availability, the use of inhibitors derived from pharmaceutical drugs during the corrosive pickling process are one of the most effective methods to prevent metal from corroding in acidic environments [5].

Omeprazole (OMP) is an outdated drug that was used in this study to inhibit the corrosion of Al-Mg-Si Alloy in an H_2SO_4 (0.5 M) solution. Among the most important characteristics of this component, which is environmentally friendly and non-harmful to human health, as well as its cost-effectiveness, is that it is low and simple to manufacture with a high degree of purity, and its chemical composition reveals that it contains many active sites that aid in the adsorption process [6]. The current study aims to investigate the inhibition effect of an eco-friendly compound on Al-Mg-Si alloy in H_2SO_4 (0.5 M) based on the previously cited literature. The

corrosion inhibition performance of OMP was determined by various electrochemical approaches [potentiodynamic polarization (PDP) and electrochemical impedance spectroscopy (EIS)].

Additionally, both with and without inhibitory molecules, the effect of temperature on the dissolution of the Al-Mg-Si alloy was investigated. The parameters of thermodynamics were computed and explained. The corresponding adsorption and protective mechanisms at the molecular and atomic levels were explored through the Langmuir, SEM, EDS, and XRD. It is believed that this study could offer interesting conceptions in the development and practical application of green inhibitors.

2. EXPERIMENTAL SECTION

2.1. Material preparation and solutions

Al-Mg-Si alloy with a chemical composition measured in weight percent was the metal employed in this study: 0.4-0.9Mg, 0.3-0.7Si, Al balance. The test materials were polished to a 1200-grade finish with various emery papers before exposure, then cleaned with acetone, washed with bidistilled water, and thoroughly dried [7]. The molecular structure of OMP **(**$C_{17}H_{19}N_3O_3S$**)** is depicted in Figure 1. The concentration of OMP (OMP) ranged from 0.3 g/L to 1.5 g/L in 0.5 M H_2SO_4 solution.

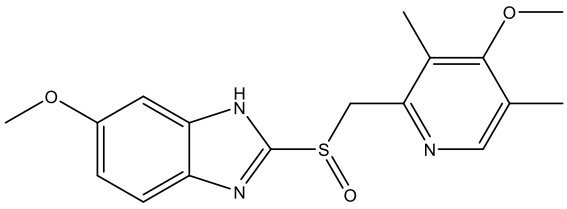

Figure 1. The molecular structure of OMP

2.2. Electrochemical Measurements

All experiments were carried out using an Origaflex Potentiostat/Galvanostat (OGF05A) controlled by a desktop computer running Origamaster5 software; a three-electrode cell set: The working electrode was an Al-Mg-Si Alloy aluminum electrode with a surface area of 1 cm^2 which was immersed in the electrolyte solution for 30 minutes at open circuit potential (E_{ocp}). The auxiliary electrode, the counter electrode, was Cl-(3 M)/Hg_2Cl_2(s)/Hg (L)/Pt.

Polarization curves were captured between the potential ranges of "-1.20 to -0.25 V" at a scan rate of 5×10^{-4} V/s. Using an amplitude of 0.01 V, a density of 20 steps per decade, and a frequency range of 0.1×10^{6} Hz to 0.1×10^{-4} Hz, electrochemical impedance spectroscopy (EIS) measurements were performed. All of the gathered data were evaluated

using the equivalent circuit program EC-Lab. However, for the sake of repeatability, the tests were repeated three times. The polarization resistance in the non-existence (R_p) and existence (R_{p-inh}) of the OMP inhibitor can be used to predict the inhibitory impact of the test molecule by means of the EIS information, as described in equation (1):

$$\eta_{EIS}(\%) = \frac{R_{p-inh} - R_p}{R_{p-inh}} \times 100 \quad (1)$$

The equation may be used to calculate the PDP inhibition efficiency (%) from the corrosion potential obtained from the Tafel line segments of the anodic and cathodic curves to yield i_{corr} (in the absence of OMP concentration) and i_{corr}^{inh} (in the presence of the various concentration of OMP) (2):

$$\eta_{PDP}(\%) = \frac{i_{corr} - i_{corr}^{inh}}{i_{corr}} \times 100 \quad (2)$$

2.3. UV–Vis spectroscopy

In surface treatments, the electrode was scraped with progressively finer emery paper grades up to 1200 before being cleaned with bi-distilled water, degreased with an alkaline solution, and dried. At ambient temperature, the solutions' spectral absorption was determined using a UV-Vis spectrophotometer (Jasco model V-730). For the UV-Vis spectrum, the spectra were obtained between 200 and 800 nm.

2.4. SEM-EDS analysis and X-ray diffraction

After 24 hours, 48 hours, and 72 hours of immersion in 0.5 M H_2SO_4, Al-Mg-Si alloy surface specimens were subjected to the optimal inhibitor concentration and the absence of the inhibitor, respectively, using a Shimadzu 6100 diffractometer. Measurements were conducted with CuK ((λ = 1.541838), an angular range of 30° < 2θ < 80°, and a sweep rate of 2 deg/min. The morphological and specimen estimation were completed by means of a scanning electron microscope with X-ray detection. A JEOL-Model JSM-IT 100 with an acceleration energy of 2×10^4 V was used for the measurements.

3. RESULTS AND DISCUSSION

3.1. Electrochemical measurements

3.1.1. Open circuit potential

Figure 2 shows the progression of the open circuit potential (E_{ocp}) over time for the dissolution of an Al-Mg-Si alloy in a 0.5 M H_2SO_4 solution without and with various concentrations of OMP. The potential-time curve shifted to the positive side in the absence

of a corrosion inhibitor. Because of its highly active nature, the passive aluminum oxide film formed quickly. After a while, the E_{OCP} became negative. This pattern is attributed to the dissolution of the passive oxide film due to sulfate ion adsorption (SO_4^{2-}). In the presence of the inhibitor, E_{OCP} increased towards positive values with rising OMP concentrations within 30 minutes, encouraging the creation of an aluminum oxide and OMP film on the metal surface. This behavior could be explained by the stable adsorption of OMP molecules on the surface of the Al-Mg-Si Alloy sample.

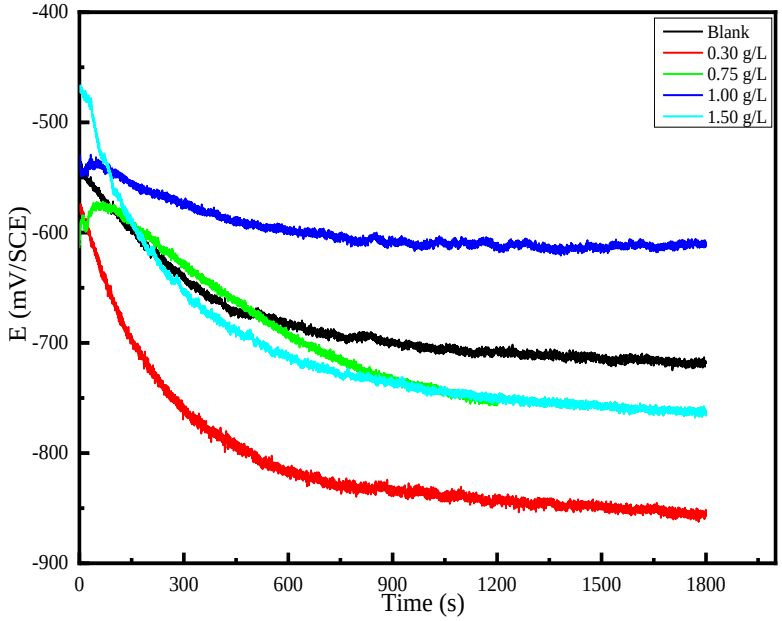

Figure 2. OCP values of Al-Mg-Si Alloy in 0.5 M H_2SO_4 at diverse concentrations of OMP

3.1.2. Concentration effect of OMP by potentiodynamic polarization

Figure 3 shows the plotted potentiodynamic polarization curves for Al-Mg-Si Alloy in 0.5 M H_2SO_4 with inhibitor concentrations ranging from 0.3 g/L to 1.5 g/L at 298 K. The electrochemical parameters and the inhibitory efficiency $\eta_{PDP}(\%)$ derived from the polarization experiments are summarized in Table 1.

Table 1. Electrochemical parameters obtained from potentiodynamic polarization curves of Al-Mg-Si Alloy in 0.5M H_2SO_4 solution containing different concentrations of OMP

Conc	$-E_{corr}$ (mV_{SCE})	i_{corr} ($\mu A/cm^2$)	β_a (mV/dec)	$-\beta_c$ (mV/dec)	$\eta_{PDP}(\%)$
Blank	738.0	102.0	301.4	224.3	----
0.3 g/L	906.9	49.8	359.5	292.5	51.2
0.7 g/L	805.6	27.0	331.5	287.3	73.5
1.0 g/L	905.0	18.1	414.3	321.5	82.2
1.5 g/L	864.8	9.5	287.0	237.9	90.7

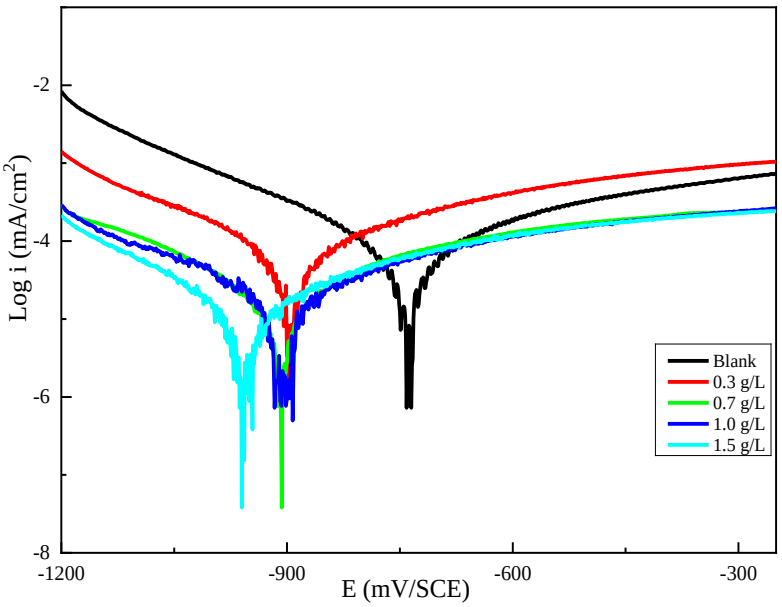

Figure 3. PDP curves for Al-Mg-Si alloy corrosion in 0.5 M H_2SO_4 and at various OMP concentrations

The inhibitor raises both the anodic and cathodic overvoltage, but its effect on the cathodic side is much subtler. In fact, the anodic reaction occurs when the metal dissolves in a strongly acidic solution, allowing aluminum ions to move from the metal surface into the solution. While the cathodic region's reaction involves the release of hydrogen protons, which contributes to the production of H_2, an inhibitor's role is to obstruct either the cathodic or anodic reaction, or both [8,9].

The anodic and cathodic sets reactions in according to the following equation:

$$Al \rightarrow Al^{3+} + 3e^{-} \quad (3)$$

$$2H^{+} + 2e^{-} \rightarrow 2H_{ads} \rightarrow H_2 \quad (4)$$

The Tafel lines are parallel in the cathodic domain (Figure 3), and the cathodic Tafel slopes (β_c) in Table 1 are almost unchanged, indicating that activation controls the reduction of hydrogen protons on the metal surface; additionally, OMP does not affect the hydrogen release mechanism. Table 1 shows that the inclusion of OMP reduces the anodic and cathodic current densities, increasing the inhibition efficiency to 90.7%. Additionally, it was discovered that the addition of the inhibitor somewhat altered the Tafel line slopes of the anodic (β_a) and cathodic (β_c). These findings demonstrated that this inhibitor simply prevents the surface area from becoming accessible.

These results imply that the inhibitor simply blocks the accessible surface in order to function. This indicates that the inhibitor only partially inactivates the surface with respect to the corrosive medium while having no effect on the Al-Mg-Si Alloy's dissolution mechanism [10,11]. Additionally, in the presence of OMP, the corrosion potential, E_{corr}, moves into the cathodic area. However, the shift in two concentrations is less than 85 mV,

which is the generally acknowledged cutoff point for the E_{corr} shift at which an inhibitor can be classified as solely anodic or cathodic[12,13]. The alteration in E_{corr} values may be attributed to a mixed type of inhibition, in which the inhibitor to a varying extent effectively regulates both the hydrogen evolution at the cathode and the metal dissolution at the anode; the inhibitor's main regulation, however, is on the cathodic hydrogen evolution reaction, which reduces the rate of corrosion overall [14]. Additionally, to these results, the considerable reduction in corrosion current density, i_{corr}, in the presence of OMP demonstrates a significantly slowed corrosion process at the optimal OMP concentration of 1.5 g/L in 0.5 M sulfuric acid.

3.1.3. Concentration effect of OMP by Electrochemical impedance spectroscopy (EIS)

The impedance behaviour as a function of inhibitor concentration was investigated using the electrochemical analysis software EC-lab. this study was represented graphically by Nyquist (Figure 4a) and Bodes (Figure 4b) plots.

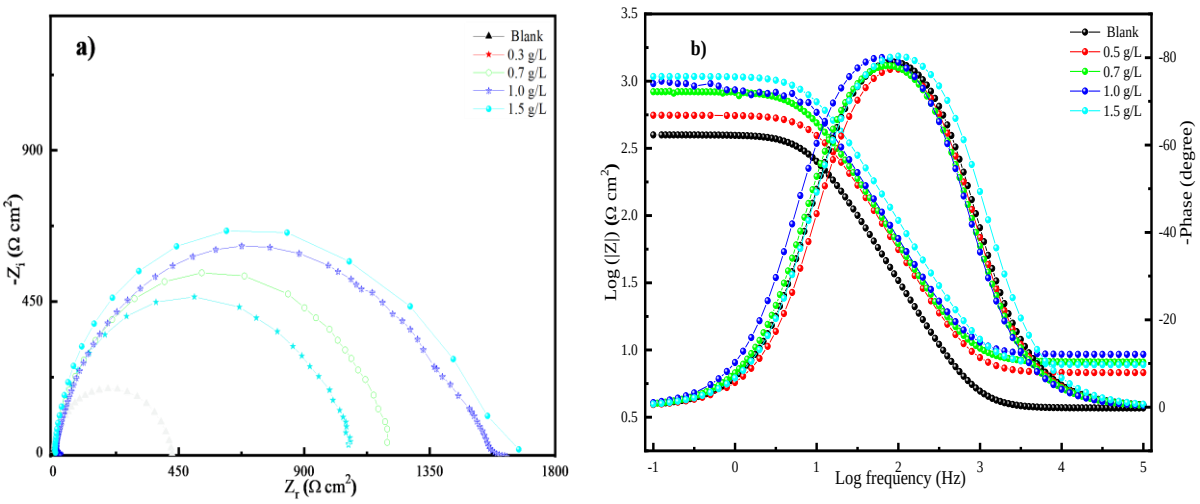

Figure 4. The Nyquist plots(a), bode-module -phase(b) plots for aluminum in 0.5 M H_2SO_4 solution containing various concentrations of Omeprazole (OMP) at 298 K

The Nyquist complex Figure 4a plot in each case shows only a single depressed capacitive semicircle, implying a unique relaxation process with a single time constant at the electrode/electrolyte interface. The depression observed in the semicircle is attributed to the electrode surface's heterogeneity and roughness [15]. The Nyquist plots assume that the polarization resistance R_p governs the corrosion of Al-Mg-Si Alloy in an H_2SO_4 solution. Furthermore, the diameter of the capacitive loop in the presence of the utilized inhibitor is greater than that of the blank solution and rises with inhibitor concentration [16]. This results in improved inhibition performance, which might be due to greater surface covering by the inhibitor molecules. This feature inhibits the aggressive solution's direct access to the metal

surface, so preventing the metal dissolution process. Furthermore, The C_{dl} values diminish as the inhibitor concentration. This seems to be attributed towards the adsorbed inhibitor molecules progressively replacing the water molecules in the double layer, forming an adherent film on the metal surface and lowering the local dielectric constant of the metal-solution interface[17]. However, the following might explain the inhibitor's rather strong performance: On the aluminum oxide (Al_2O_3) coating develops naturally; this film protects the metal until it is largely dissolved in the acid solution[18,19].

Figure 4b of the Bode plots shows the existence of a unique time constant at all inhibitor concentrations. It further indicates that the phase angle depression at the relaxation frequency decreases with increasing inhibitor concentration, indicating that the capacitive response increases with increasing inhibitor concentration. Additionally, we can see from the phase angle plots that increasing the inhibitor concentration causes an absolute value of the phase angle plots to be close to 80°. This suggests that at higher concentrations, there is a higher corrosion inhibition behavior due to greater interactions between the OMP molecules and the Al-Mg-Si Alloy surface[20].

While the resultant semicircular shape provides different levels of corrosion protection, detailed analysis required adjustment of the data obtained with the equivalent electrical circuit. Based on the proposed equivalent circuit (EEC) presented in

Figure 5, the EIS data were simulated.

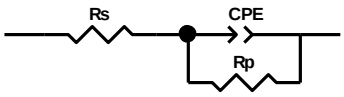

Figure 5. Equivalent circuit for the metal–acid interface

The solution resistance R_s (Ω cm^2), and the polarization resistance R_p (Ω cm^2) were generated by fitting the data with a single constant equivalent circuit, and CPE is a constant phase element representing the double layer capacitance of the Metal-solution interface, introduced to compensate for system heterogeneity caused by surface roughness, inhibitor adsorption, porous layer formation, and so on. The CPE impedance (Z_{CPE}) is derived from the following equation[21]:

$$Z_{CPE} = Q^{-1}\left(j\omega\right)^{-n} \quad (5)$$

where the CPE constant Q is in Ω^{-1} s^n cm^{-2}, ω is the angular frequency, j is the imaginary number ($j^2 = -1$); n is the deviation parameter ($-1 \leq n \leq +1$), which has the meaning of a phase shift.

In this case, the value of the double layer capacitance (C_{dl}) was also determined by using the follows Eq. 6:

$$C_{dl} = \sqrt[n]{Q \times R_{dl}^{1-n}} \quad (6)$$

Table 2. Impedance parameters of Al-Mg-Si Alloy in H_2SO_4 containing different concentrations of OMP

Conc	R_s (Ω cm^2)	R_p (Ω cm^2)	Q_{dl} ($\mu\Omega^{-1}$ s^n cm^2)	n	C_{dl} (μF cm^{-2})	η_{EIS} (%)
Blank	3.0	135.0	50.0	0.9980	49.5	
0.3 g/L	5.1	395.7	28.5	0.9967	28.1	65.9
0.7 g/L	8.3	751.7	21.6	0.9567	17.9	82.0
1.0 g/L	6.3	1309.2	17.3	0.9742	15.6	89.7
1.5 g/L	7.7	1 439.0	2.56	0.9880	2.40	90.6

Further investigation of the results in Table 3 reveals that when moving from the uninhibited to the inhibited solution, R_p values increase while C_{dl} values decrease, and this behavior becomes more pronounced as the inhibitor concentration increases. The reduction in C_{dl} is due to the efficient adsorption of OMP molecules onto Al-Mg-Si Alloy via water molecule replacement, which reduces the extent of the dissolution reaction. Additionally, we can see that the n values do not vary significantly even after the addition of increased inhibitor concentrations, which can aid in the prediction of the dissolving mechanism. Thus, we can infer that the charge transfer procedure controls the dissolving mechanism in both inhibited and uninhibited solutions [22]. The potentiodynamic polarization study's findings are in agreement with the findings of the EIS study.

3.1.3. Temperature Effect by potentiodynamic polarization

The inhibitory behaviour of OMP at its optimum concentration (1.5 g/L) was tested at different temperatures (298, 303, 313, 323, and 333 K) using PDP measurements and the results are shown in Figure 6**.** Besides, Table 3 reveals the measured corrosion parameter values, including E_{corr}, i_{corr}, and η_{PDP} (%) which indicate respectively, the corrosion potential, the corrosion current density, and the inhibition efficiency. Because the OMP molecule adsorbed on the metal surface desorbs at high temperatures, the i_{corr} values in the presence of OMP increase somewhat as temperature rises compared to the virgin solution, which increases significantly. As a result, the efficiency of OMP inhibition significantly decreases.

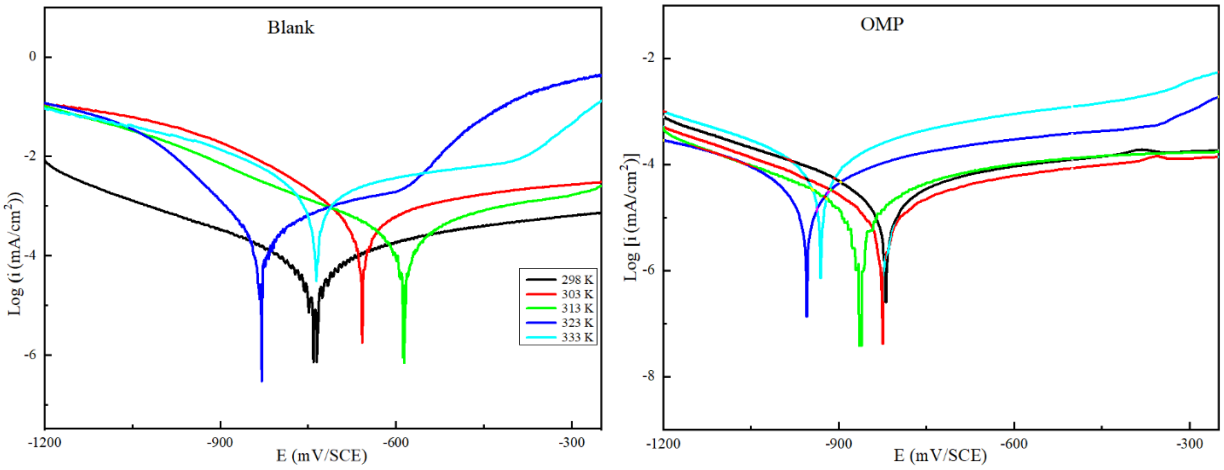

Figure 6. PDP curves for corrosion of Al-Mg-Si Alloy in 0.5 M H_2SO_4 electrolyte with and without OMP at diverse temperatures

Table 3. Corrosion characteristics for Al-Mg-Si alloy in 0.5 M H_2SO_4 solution with and without the addition of OMP at various temperatures determined from PDP curves

Medium	Temp (K)	$-E_{corr}$ (mV_{SCE})	i_{corr} ($\mu A/cm^2$)	$\eta_{PDP}(\%)$
Blank	298	738.0	102.0	
	303	586.7	116.8	
	313	656.4	127.6	
	323	649.3	160.9	
	333	739.7	469.9	
1.5 g/L	298	864.0	9.5	90.7
	303	821.3	15.4	86.8
	313	817.2	28.7	77.5
	323	926.8	56.8	64.7
	333	951.6	178.2	62.1

Here, we can demonstrate the effect of temperature by applying the Arrhenius equations and the transition state[23]:

$$i_{corr} = A\exp\left(\frac{-E_a}{RT}\right) \quad (6)$$

$$i_{corr} = \frac{R\times T}{N\times h}\exp\left(\frac{\Delta S_a}{R}\right)\exp\left(\frac{-\Delta H_a}{RT}\right) \quad (7)$$

where, A, ΔS_a, ΔH_a, N, h, and E_a are respectively, the pre-exponential factor, the entropy of activation, the enthalpy, the Avogadro number the Planck constant, and the activation energy.

Based on the Arrhenius equation (6) one can determine the activation energy (E_a) by plotting different values of ln (i_{corr}) as a function of 1000/T, one can thus calculate E_a (Figure 7-a). where a straight line is given by ln (i_{corr}/T) as a function of (1000/T) (Figure 7-b). A straight line is given by ln (i_{corr})/T as a function of (1000/T) (Figure 7-b) Its slope is (-ΔH_a / R), and its intersection with the axis ln (i_{corr})/T gives the parameter ΔS_a.

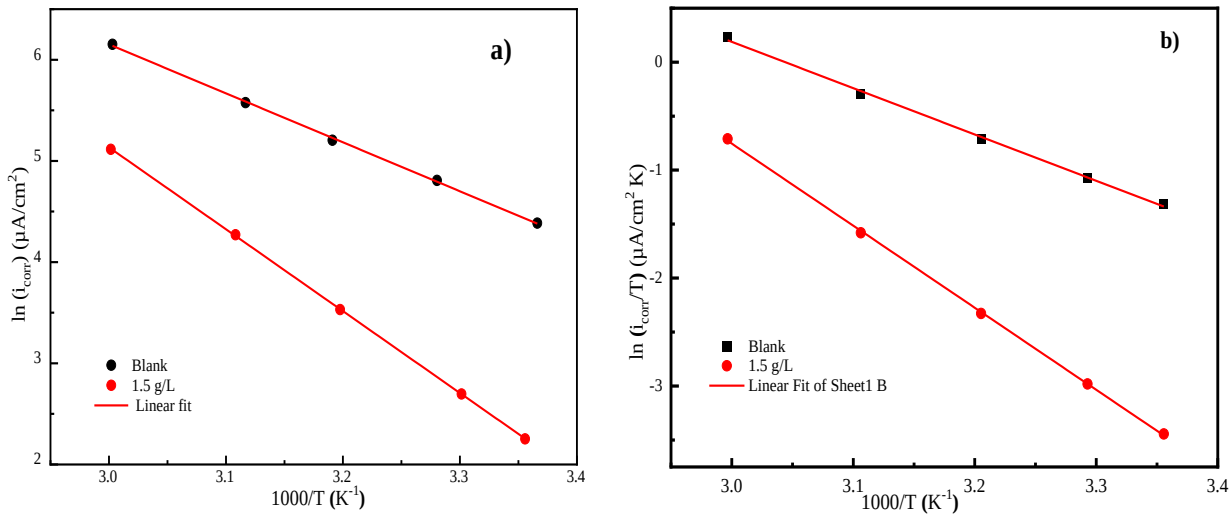

Figure 7. Traces of ln (i_{corr}) versus 1000/T and ln i_{corr} /T versus 1000/T for Al-Mg-Si Alloy without and with OMP at its optimum concentration at different temperatures

Table 4. The parameters of activation of dissolved Al-Mg-Si in a virgin solution and the optimum concentration of the OMP at varying temperature

Medium	E_a (kJ mol^{-1})	ΔH_a (kJ mol^{-1})	-ΔS_a (J mol^{-1} K^{-1})
Blank	40.26	37.64	89.03
OMP + H_2SO_4 (0.5 M)	67.53	64.91	14.18

The results show that in the presence of OMP, E_a values are higher than in the absence, suggesting that the physisorption mechanism through which OMP adsorbs happens spontaneously at the first stages of metal-inhibitor interactions [24].

Despite this, we discovered that the activation enthalpy ΔH_a values are positive both in the absence of the optimal inhibitor concentration and in the presence of the virgin acid solution, indicating that the process is endothermic and that an energy barrier has formed in the presence of OMP. Under identical conditions, negative activation entropy ΔS_a values emerge from the association of the inhibitor molecules rather than their dissociation. A

higher degree of disorder (or unpredictability) in the reactants' reaction to the activated complex is shown by the fact that the value of ΔS_a is more significant in the existence of OMP than it is in the non-existence [25].

3.2. Adsorption study

The molecular adsorption of the corrosion inhibitor on the metal surface is primarily responsible for the inhibitory effect on the corrosion of metallic materials. When in contact with an aqueous solution, a metal surface becomes saturated with water molecules; however, when a corrosion inhibitor is present, these molecules push the adsorbed water out of the way. When water is replaced with OMP molecules, the active regions of the metal surface where corrosion processes occur are blocked.

The Langmuir model, which is the most often used adsorption isotherm model, is employed in this study to analyze the adsorption behavior of OMP. Thus, Langmuir adsorption isotherm can be obtained by the linear regression of C_{inh}/θ vs. C_{inh} as shown in Figure 8. The equation of this model is the following

$$\frac{C_{inh}}{\theta} = \frac{1}{K_{ads}} + C_{inh} \tag{8}$$

where K_{ads} is the adsorption equilibrium constant, C_{inh} is the inhibitor concentration, and θ represents the covered surface fraction.

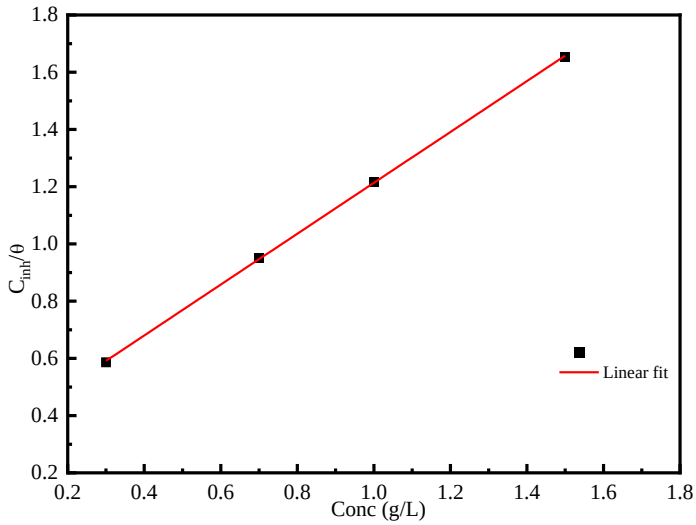

Figure 8. Langmuir adsorption isotherm of OMPe on the Al-Mg-Si Alloy surface at 298 K.

The values of the two K_{ads} obtained from the inverse of the Langmuir isotherm intercept and the Gibbs adsorption free energy ΔG^0_{ads} calculated from the following equation (9):

$$\Delta G^0_{ads} = -RT \ln\left(C_{H_2O} \times K_{ads}\right) \tag{9}$$

The values R, C_{H2O}, and T stand for universal gas constant, pure water concentration in the solution, and temperature (K) (R = 8.314 J mol^{-1} K^{-1} and C_{H2O} = 1000 g L^{-1}), respectively. The thermodynamic parameters extracted from the above figure are gathered in Table 6.

Table 5. Parameter of Langmuir adsorption isotherm for the OMP inhibitor

	K_{ads} (L g^{-1})	R^2	ΔG^0_{ads} (kJ mol^{-1})
Inhibitor	3232.82	0.9998	-37.1627

In general, the interaction values between charged molecules and the charged metal of ΔG^0_{ads} up to -20 kJ/mol are consistent with electrostatics and typically involve the sharing or transfer of electrons from the inhibitor molecules (physical adsorption) while those more negative than -40 kJ/mol on the metal surface to produce a type of coordinated bond (chemisorption).

Physical adsorption (electrostatic) naturally occurs when the effectiveness of inhibition decreases with increasing temperature (while chemical adsorption occurs when the efficacy of inhibition increases with increasing temperature. The presence of hetero atoms like oxygen, nitrogen, and aromatic rings with π-bonds in the OME molecules, which act as adsorption centers on the metal surface, is the primary cause of the inhibitor's inhibitory activity. The mechanism of substitutional adsorption between the organic molecule in the aqueous solution and the water molecules adsorbed on the metal surface is assumed to be responsible for the adsorption of an organic adsorbate on a metal surface:

$$Org_{(sol)} + xH_2O_{(ads)} \rightarrow Org_{(ads)} + H_2O_{(sol)} \quad (10)$$

x being the size ratio, the adsorption of inhibitor compounds can be divided into two main categories: physical and chemical interactions, each of which precisely describes the quantity of water molecules that an organic adsorbate molecule replaces. It is influenced by the nature and charge of the metal, the chemical composition of the inhibitor, and the kind of electrolyte [26].

The measured value of ΔG^0_{ads} is -37.16 kJ mol^{-1}, and this energy is related to the interactions between the metal's charge and the charges on the inhibitor molecules (physisorption). This adsorption can be attributed to the adhesion of the molecule to the Al-Mg-Si Alloy surface by a chemisorption mechanism with physisorption [27].

3.3. UV–Vis Absorption Spectroscopy

The solution's UV-Vis spectroscopy allowed for further interpretation of the inhibition effect. Figure 9 depicts the UV-Vis spectroscopy of the solution after 2 days (48 h) of immersion in the metal; the black line corresponds to the 0.5 M H_2SO_4 solution (Blank), and the red line corresponds to the 0.5 M H_2SO_4 solution with 1.5 g/L inhibitor (OMP) and the bleu one attributed to the sample immersed in 0.5 M H_2SO_4 with the addition of OMP at the optimum concentration.

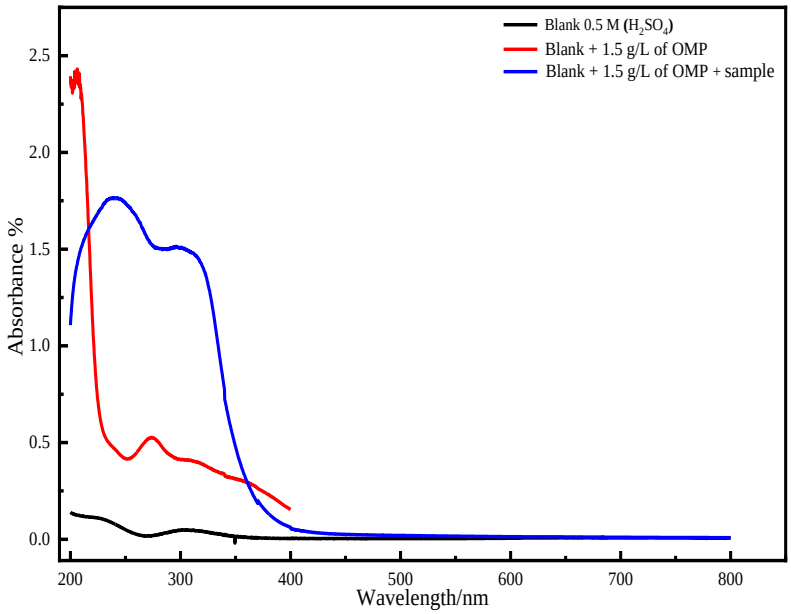

Figure 9. UV-Vis absorption spectroscopy of the 0.5 M H_2SO_4 electrolyte (Blank with and without the addition of 1.5 g/L OMP) after 48 hours of immersion time of Al-Mg-Si Alloy at room temperature

The UV-visible spectra show an intense band at λ_{max}=206 nm with a higher absorbance attributed to the dissolution of OMP molecules in the blank solution which present the effect of the environment on the transitions; however, after 48 hours of immersion of Al-Mg-Si Alloy in the solution containing 1.5 g/L of OMP, we can detect the appearance of such an intense ring at λ_{max} = 240 nm contributed to the hypochromic effect (π-π*) and a second band at λ_{max} = 306 nm attributed to the bathochromic(n-π*) and a modification of absorbance related to the medium saturated in H_2SO_4 and the inhibitor (existence of auxochrome groups) [28,29]. After 48 hours, the inhibitor provides some corrosion protection against the oxidation by-product. A passive Al_2O_3 film is formed when oxygen or aluminum atoms from the substrate mix and diffuse to the surface [30]. The development of the Al_2O_3 protective film, confirmed by XRD and SEM/ EDS techniques, can be assisted by the adsorption of OMP molecules on the surface of Al-Mg-Si Alloy formed by oxidation [31].

3.4. SEM-EDS analysis and X-ray diffraction

3.4.1. SEM-EDS analysis

Figure 10-a shows SEM/EDS pictures of the surface of Al-Mg-Si Alloy after specimens were submerged in a 0.5 M H_2SO_4 solution for 48 h in the absence of the inhibitor. The surface of the alloy was severely damaged and became porous and rough with large holes of varied sizes. Using the development of SO3 and Al2O3 oxides, which were confirmed with XRD in the following paragraph, the EDS spectrum in Figure 10-b described the characteristic signals of aluminum in addition to other elements, such oxygen and sulfur, which are frequently seen as corrosion products of aluminum in sulfuric acid. Because of the breakdown of the protective layer formed on the metal surface, the corrosion rate of Al-Mg-Si Alloy Al increases continuously. This breakage is regarded as the start of localized corrosion damage [32]. Furthermore, the passivity breakdown potential increases in alkaline conditions, while the acidic solution weakens the passive film [33,34].

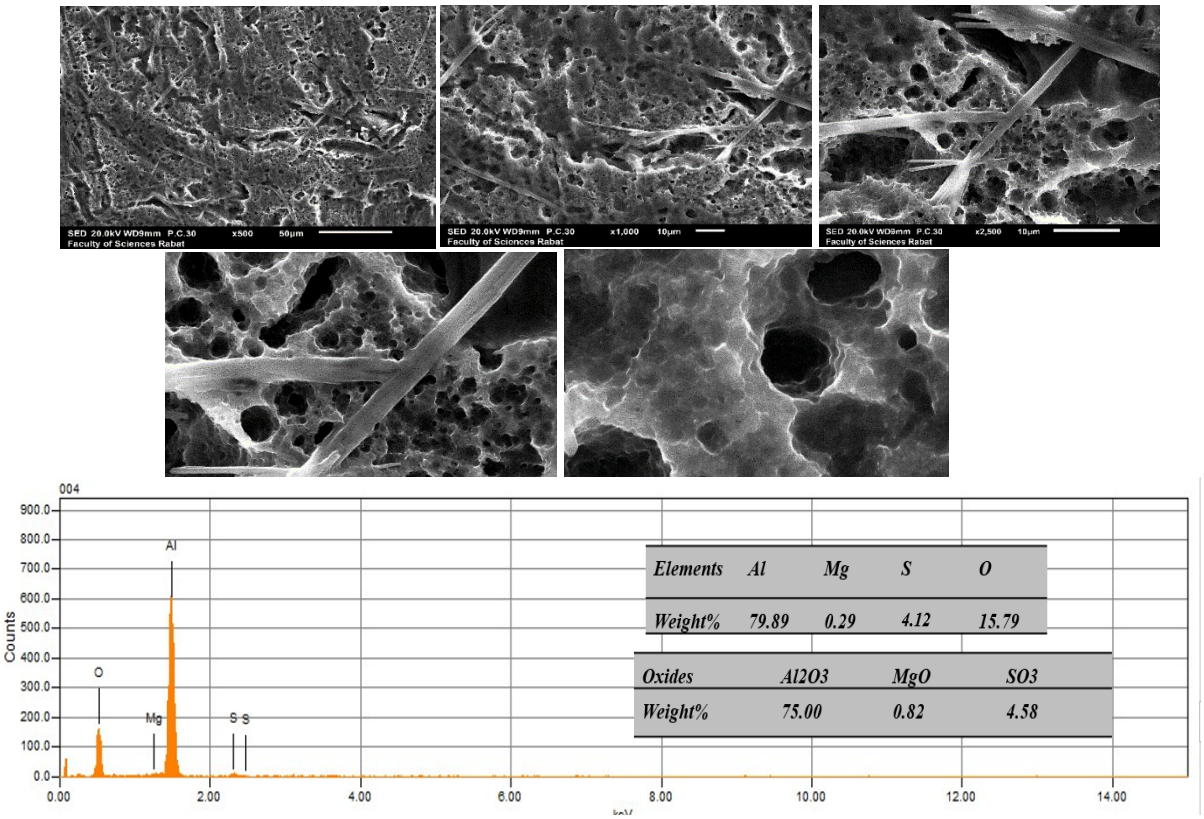

Figure 10. a) SEM images of Al-Mg-Si Alloy that was immersed for 48 h in 0.5 M H_2SO_4; **b)** EDS of Al-Mg-Si Alloy immersed in 0.5 M H_2SO_4 at 48 h

Similarly, SEM/EDS images of the pure Al surface after immersion in a 0.5 M H_2SO_4 solution containing 1.5 g/L OMP for 48 h (Figures 11a & b). The SEM micrographs strongly indicate that the addition of OMP to the acidic solution coated the surface of the Al-Mg-Si

alloy, that further enhanced the metal's corrosion resistance by re-passivating the protective barrier on the metal surface. The EDS spectrum shows the proportion of passive film formation on the metal surface due to the presence of OMP, which improves the protection of the metal against corrosion caused by alkaline solution and indeed the reduction of corrosion products on the metal surface might have been caused by the adsorption through several elements in the OMP on the aluminum surface which typically protected the metal surface from the attack of the aggressive environment.

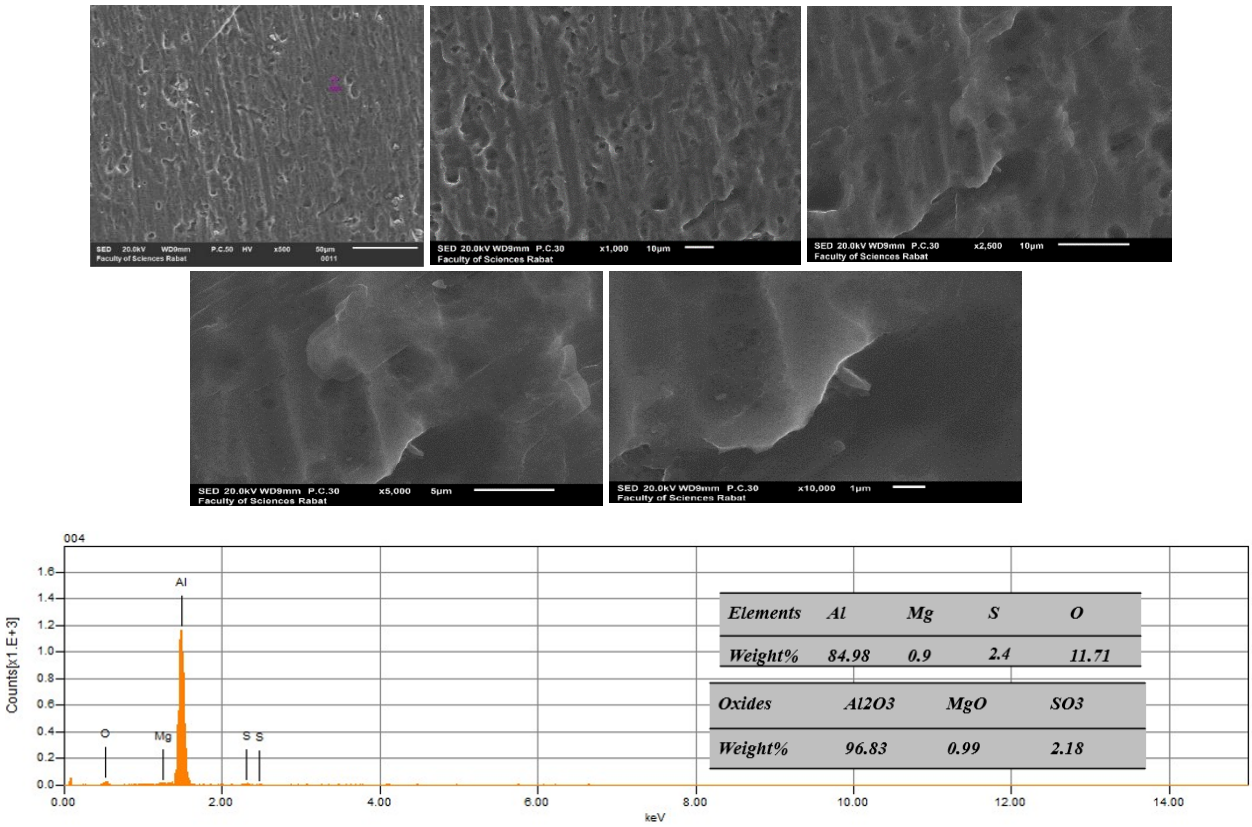

Figure 11. a) SEM images of Al-Mg-Si Alloy that was immersed for 48 h in 0.5M H_2SO_4 with the addition of 1.5 g/L of OMP; **b)** EDS images of Al-Mg-Si Alloy that was immersed for 48 h in 0.5M H_2SO_4 with the addition of 1.5g/L of OMP.

3.4.2. X-ray diffraction analysis

Figure 12 shows the XRD diffraction spectra for samples immersed in 0.5 M H_2SO_4 with and without OMP at 48 h. The patterns above for the uninhibited and inhibited Al-Mg-Si alloy show the same peaks at 2θ = 39.3, 45.5, 65.8, with different intensity. These peaks correspond to gibbsite [γ-$Al(OH)_3$], bayerite [[α-$Al(OH)_3$], alumina (Al_2O_3) [35]. On the other hand, the intensity of the peaks associated with alumina increased with the addition of OMP compared to a non-inhibited surface, indicating a better efficiency of the inhibitor adsorbed on the metal

surface and promoting the new formation of Al_2O_3, which increases the corrosion resistance [36].

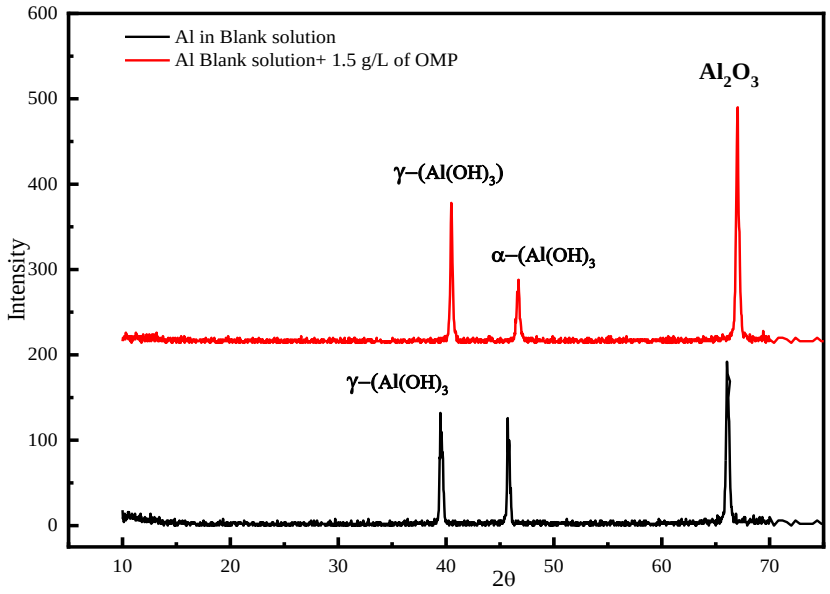

Figure 12. XRD patterns of corrosion Product formed on the Al-Mg-Si alloy surface after 48 h in the existence of 1.5 g/L OMP and in it's the non-existence

4. CONCLUSION

The inhibitor inhibits corrosion of Al-Mg-Si in 0.5 M H_2SO_4 solution with good efficiency, with a notable rise in inhibition effectiveness with increasing inhibitor concentration (1.5 g/L). The OMP inhibitor behaved as a mixed type inhibitor, according to polarization experiments. According to adsorption studies, the Langmuir adsorption model is followed by inhibitor adsorption on metal surfaces. According to SEM/EDS and XRD measurements, the inhibitor's increased activation energy compared to the blank suggests the creation of a protective barrier on the metal surface Al_2O_3. Negative values indicate implying that the inhibitor was highly adsorbed on the aluminum surface. The results point to a chemisorption process with physisorption.

REFERENCES

[1] R.U. Din, K. Bordo, M.S. Jellesen, and R. Ambat, Surf. Coatings Technol. 276 (2015) 106.

[2] A.A. Khadom, and S.N. Farhan, Corros. Rev. 36 (2018) 267.

[3] H. Zarrok, A. Zarrouk, R. Salghi, H. Oudda, B. Hammouti, M. Ebn Touhami, M. Bouachrinee, and O.H. Pucci, Port. Electrochim. Acta 30 (2012) 405.

[4] F. Bentiss, M. Traisnel, N. Chaibi, B. Mernari, H. Vezin, and M. Lagrenée, Corros. Sci. 44 (2002) 2271.

[5] Z. Tao, W. He, S. Wang, S. Zhang, and G. Zhou, J. Mater. Eng. Perform. 22 (2013) 774.
[6] X. Li, S. Deng, H. Fu, and T. Li, Electrochim. Acta 54 (2009) 4089.
[7] ASTM G31 – 72, ASTM G31: Standard Practice for Laboratory Immersion Corrosion Testing of Metals, ASTM Int. i (2004) 5.
[8] N. Soltani, N. Tavakkoli, M. Khayatkashani, M.R. Jalali, and A. Mosavizade, Corros. Sci. 62 (2012) 122.
[9] A. Ennouri, A. Lamiri, and M. Essahli, Port. Electrochim. Acta 35 (2017) 279.
[10] M.S. Uwineza, M. Essahli, and A. Lamiri, Port. Electrochim. Acta. 34 (2016) 53.
[11] S.C. Nwanonenyi, H.C. Obasi, E.E. Oguzie, I.C. Chukwujike, and C.K. Anyiam, J. Bio-Tribo-Corrosion. 3 (2017).
[12] M.M. Rguiti, M. Chadili, B. El Ibrahimi, A. Baddouh, L. Bazzi, M. Hilali, and L. Bazzi, Moroccan J. Chem. 6 (2018) 307.
[13] M.R. Laamaria, J. benzakoura, F. Berrekhis, M. Bakassec, and D. Villemind, J. Mater. Environ. Sci. 3 (2012) 485.
[14] I.O. Arukalam, I.O. Madu, N.T. Ijomah, C.M. Ewulonu, and G.N. Onyeagoro, J. Mater. 2014 (2014) 1.
[15] A. Batah, M. Belkhaouda, L. Bammou, A. Anejjar, R. Salghi, and B. Hammouti, Moroccan J. Chem. 5 (2017) 580.
[16] M.H. Sliem, N.M. El Basiony, E.G. Zaki, M.A. Sharaf, and A.M. Abdullah, Electroanalysis. 32 (2020) 3145.
[17] M.A. Hegazy, M. Abdallah, M.K. Awad, and M. Rezk, Corros. Sci. 81 (2014) 54.
[18] P. Arellanes-Lozada, O. Olivares-Xometl, D. Guzmán-Lucero, N. V. Likhanova, M.A. Domínguez-Aguilar, I. V. Lijanova, and E. Arce-Estrada, Materials (Basel) 7 (2014) 5711.
[19] Y. Yang, A. Kushima, W. Han, H. Xin, and J. Li, Nano Lett. 18 (2018) 2492.
[20] T.A. Yousef, R.K. Hussein, A.G. Alhamzani, A.T. Al-Enazi, M.B. AL-Osimi, and M.M. Abou-Krisha, Metals (Basel) 12 (2022).
[21] H. Ashassi-Sorkhabi, D. Seifzadeh, and M.G. Hosseini, Corros. Sci. 50 (2008) 3363.
[22] A. Chaouiki, M. Chafiq, A.H. Al-Moubaraki, M. Bakhouch, M. El Yazidi, and Y.G. Ko, Arab. J. Chem. 15 (2022) 104323.
[23] A.S. Yaro, R.K. Wael, and A.A. Khadom, J. Univ. Chem. Technol. Metall. 45 (2010) 443.
[24] E.E. Oguzie, C. Unaegbu, C.N. Ogukwe, B.N. Okolue, and A.I. Onuchukwu, Mater. Chem. Phys. 84 (2004) 363.
[25] S. Manimegalai, and P. Manjula, J. Mater. Environ. Sci. 6 (2015) 1629.
[26] A. Dąbrowski, Adv. Colloid Interface Sci. 93 (2001) 135.
[27] J.D. Talati, and D.K. Gandhi, Corr. Sci. 23 (1983) 1315.
[28] V. Kothekar, Basic UV-Vis Theory, Concepts and Applications Basic UV-Vis Theory,

Concepts and Applications, Protocol. (2012) 1.
[29] N.O. Obi-Egbedi, and I.B. Obot, Arab. J. Chem. 5 (2012) 121.
[30] C.S. Proença, B. Serrano, J. Correia, and M.E.M. Araújo, Metals (Basel) 12 (2022).
[31] G. Kordas, Corros. Mater. Degrad. 3 (2022) 376.
[32] T.J.R. Leclere, A.J. Davenport, and R.C. Newman, Corrosion 63 (2007) 338.
[33] S. Zhang, C. Sun, J. Di, and Y. Tan, Metals (Basel) 10 (2020) 1.
[34] J. Kruger, J.R. Ambrose, and T. Kodama, NBSIR 75-916 The Role of Passive Film Growth Kinetics and Properties in Stress Corrosion and Crevice Corrosion Susceptibility, (1975) 83.
[35] R.E. Azooz, J. Electrochem. Sci. Eng. 6 (2016) 235.
[36] D. Wang, D. Yang, D. Zhang, K. Li, L. Gao, and T. Lin, Appl. Surf. Sci. 357 (2015) 2176.